



Loss of Nanoparticles in a Particulate Matter Sampling System Applied for Environmental Ultrafine Particle Measurements

Julian Zoller¹ · Jonas Gulden¹ · Jörg Meyer¹ · Achim Dittler¹

Received: 19 September 2019 / Revised: 29 January 2020 / Accepted: 14 February 2020 / Published online: 4 March 2020
© The Author(s) 2020

Abstract

Current air monitoring networks consist of many measuring stations equipped with sampling systems for the measurement of PM_{2.5} and PM₁₀ particulate matter. To measure the quantity of particulate matter, the sample air flow is fed to the measuring device through a sampling system. In Baden Württemberg, but also across a wide area in Germany, these sampling systems consist of a Sigma-2-Sampling Head (manufacturer Palas GmbH) and an Intelligent Aerosol Drying System (IADS, manufacturer Palas GmbH). To investigate the suitability of these two common components for sampling of ultrafine particles (< 100 nm), the particle loss inside a sampling system consisting of a Sigma-2-Sampling Head, an IADS, and an additional nafion-dryer (MD-700-24S-1, manufacturer Perma Pure LLC) is measured in this study. A low sampling flow rate of only 0.9 l/min was employed to reduce energy consumption, complexity, and the cost of additional instrumentation. This sample flow rate is typical for scanning mobility particle sizers which are commonly used to measure ultrafine particles. The investigations show a 37% loss of spherical 10 nm copper particles in the used sampling system, which is higher than the allowed losses specified in DIN CEN/TS 16976 for 7 nm particles. The root cause of these losses was investigated and correlations were derived to describe the particle penetration in the sampling system.

Keywords Diffusion loss · Penetration · Ultrafine particles · Nanoparticles · Sampling

1 Introduction

1.1 Environmental Particle Sampling

Air monitoring networks measure the mass concentration of particulate matter (PM₁₀ and PM_{2.5}) around the world to evaluate air quality. The mass concentration is determined gravimetrically or with an optical particle counter under consideration of typical aerosol properties. Figure 1a shows a measuring station which is part of the air monitoring network in Baden Württemberg, Germany.

By number, most environmental aerosol particles are smaller than 100 nm. These small particles are called

ultrafine particles and provide only a small share in the commonly measured mass concentrations (PM₁₀ and PM_{2.5} values) because of their low individual mass (Stanier et al. 2004). To monitor these ultrafine particles, operators of air monitoring networks will need a sampling system for these particles. It would be advantageous if this ultrafine particle sampling system is interchangeable with the sampling systems commonly used for fine particulates, has only a small energy consumption, and does not add to much complexity in terms of flow control. In this study, the suitability of a common fine particulate sampling system is investigated for the sampling of ultrafine particles, regarding the particle loss in the sampling line. This system contains a Sigma-2-Sampling Head (manufacturer Palas GmbH) and an Intelligent Aerosol Drying System (IADS, manufacturer Palas GmbH) which are shown in Fig. 1a. The probe head prevents insects, coarse dirt, and big droplets from entering the sampling system. In this study, the IADS is used only as a long pipe that is often needed to sample at a specific height. It was not active, because reduction of relative humidity by actively increasing the gas temperature (which is what the IADS does in operation) can change particulate properties,

Electronic supplementary material The online version of this article (<https://doi.org/10.1007/s41810-020-00054-6>) contains supplementary material, which is available to authorized users.

✉ Julian Zoller
julian.zoller@kit.edu; gps@mvm.kit.edu

¹ Institute of Mechanical Process Engineering and Mechanics, Karlsruhe Institute of Technology, Straße am Forum 8, 76131 Karlsruhe, Germany

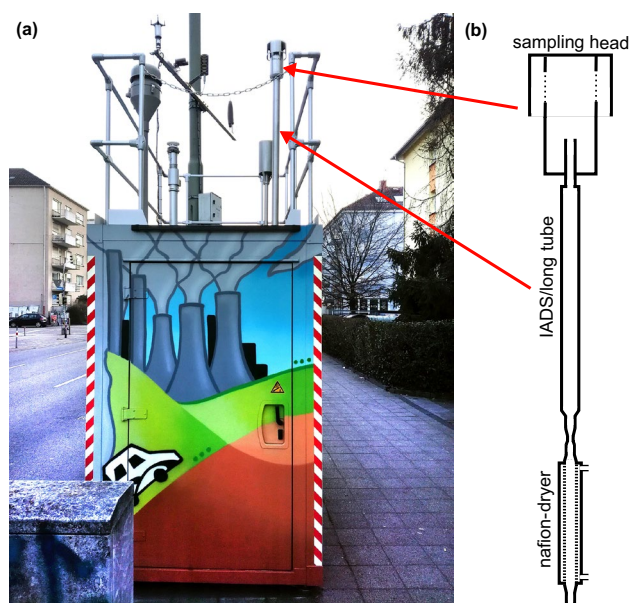


Fig. 1 Sigma-2-Sampling head and IADS on top of a measuring station in Karlsruhe Germany (a) and a schematic representation of the components forming the sampling system used in this study (b)

especially for small particles and, therefore, is not recommended in DIN CEN/TS 16976. Instead of activating the IADS, a nafion-dryer (MD-700-24S-1, manufacturer Perma Pure LLC) is used to reduce the influence of humidity on the particle size (Sinclair et al. 1974). The complete sampling system used in this study is shown schematically in Fig. 1b.

The size distribution and total concentration of ultrafine particles downstream the sampling line can be measured using a Scanning Mobility Particle Sizer (SMPS). The SMPS used in this study has a sample flow rate of 0.9 l/min (DEMC X control unit, DEMC 2000 column and ENVI-CPC 100, manufacturer Palas GmbH). To reduce energy consumption and the costs for additional instrumentation, no further flow splitter, flow control system, and pump were used in this study.

There are currently no standardized specifications for environmental measurements of ultrafine particle size distributions, which can be used to evaluate the suitability of the proposed sampling system, but DIN CEN/TS 16976 can serve as orientation. This norm specifies requirements for environmental measurements of particle number concentrations by condensation particle counters (CPC). According to DIN CEN/TS 16976, the loss of 7 nm particles in the sampling system must be lower than 30%; additionally, aerosol humidity at the CPC inlet must be lower than 40% and the flow in the sampling system must be laminar. DIN CEN/TS 16976 also suggests a possible design for a suited sampling system, which is commercially available from various manufacturers. In this design, a high volumetric flow rate through most of the sampling system up to a flow splitter just before

the measurement device minimizes diffusion losses (DIN CEN/TS 16976 2016).

This study investigates a different approach for environmental monitoring of ultrafine particles, in which components of common particulate matter sampling systems are used at a low flow rate and hence energy consumption. In this study, the losses in the proposed sampling system are measured for spherical copper particles with a size of 10, 15, 20, and 40 nm and also with different electric charge states for the flow rate of 0.9 l/min. These losses allow to evaluate the suitability of the sampling system at low flow rates for environmental ultrafine particle measurement and to gain further insight into the mechanisms causing particle loss in a real-world sampling system.

1.2 Calculation of Particle Loss

Ultrafine particles are lost in sampling systems by diffusional deposition, electrostatic dispersion, image force, and precipitation by electric fields. While diffusion loss is relevant for all small particles, electrostatic effects depend on the particle charge, number concentration, and local electric fields which are mainly defined by the surface potential of the sampling system.

The sampling system is modeled as a series of several tubes and a wire mesh, which prevents coarse particles from entering the sampling line. For tubes and wire mesh, there are several equations available in literature, which allow calculating the diffusion loss of nanoparticles.

Gormley and Kennedy derived equations for the calculation of particle penetration in laminar pipe flows (Gormley and Kennedy 1948). These equations were simplified by Hinds (1999):

$$P(x) = \frac{c_{\text{out}}(x)}{c_{\text{in}}(x)} \quad (1)$$

$$P = 1 - 5.5\mu^{2/3} + 3.77\mu \text{ for } \mu < 0.009 \quad (2)$$

$$P = 0.819 \exp(-11.5\mu) + 0.0975 \exp(-70.1\mu) \text{ for } \mu \geq 0.009. \quad (3)$$

$P(x)$ denotes the penetration of particles of the size x , $c_{\text{out}}(x)$ denotes the outlet number concentration, and $c_{\text{in}}(x)$ denotes the inlet number concentration. Equations (2) and (3) apply for all values of μ with an accuracy of 1% (Hinds 1999). The parameter μ is defined as:

$$\mu = \frac{DL}{\dot{V}}, \quad (4)$$

with the particles diffusion coefficient D , the tube length L , and the volumetric flow rate \dot{V} . For spherical particles,

the diffusion coefficient can be calculated according to the Stokes–Einstein equation (Hinds 1999):

$$D = \frac{kTC_c}{3\pi\eta x}, \quad (5)$$

with the Boltzmann constant k , the temperature T , the slip correction factor C_c , and the dynamic viscosity η . The dynamic viscosity of nitrogen can be described with a fourth-order polynomial of temperature (Kleiber and Joh 2013):

$$\frac{\eta}{\text{Pa} \cdot \text{s}} = \frac{-0.0102}{10^5} + \frac{0.74785}{10^7} \frac{T}{\text{K}} + \frac{-0.59037}{10^{10}} \left(\frac{T}{\text{K}}\right)^2 + \frac{0.0323}{10^{12}} \left(\frac{T}{\text{K}}\right)^3 + \frac{-0.00673}{10^{15}} \left(\frac{T}{\text{K}}\right)^4. \quad (6)$$

The slip correction C_c and the mean free path λ are calculated according to Hinds (1999):

$$C_c = 1 + \frac{\lambda}{x} \left(2.34 + 1.05 \exp\left(-0.39 \frac{x}{\lambda}\right) \right) \quad (7)$$

$$\lambda = \frac{RT}{\sqrt{2} N_A p \pi \sigma^2}. \quad (8)$$

R denotes the ideal gas constant, N_A denotes the Avogadro constant, p denotes the gas pressure, and σ denotes the collision diameter of the molecules. Glassman determined σ as 0.3733 nm for nitrogen at 298 K (Glassman and Harris 1952).

It is remarkable that particle penetration in the laminar diffusional regime is independent of the tube diameter at constant volumetric flow rate because of two opposing effects (Hinds 1999). On one hand, a bigger tube diameter leads to a higher distance which a particle must travel to the wall and, therefore, to a higher penetration. On the other hand, the flow velocity in the tube is reduced for bigger tube diameters, and hence, the residence time of the particles in the tube is increased which leads to a lower penetration. Both effects cancel each other out. The equations of Gormley and Kennedy were validated by Alonso experimentally (Alonso et al. 1997). Alonso used a tandem DMA configuration to generate a test aerosol of a very narrow size fraction. He measured the penetration of 2–6 nm particles, both charged and uncharged, in laminar pipe flow ($\text{Re} \approx 400$), and found a good accordance with the equations of Gormley and Kennedy.

In the turbulent regime, eddies lead to velocity components of the particles perpendicular to the main flow direction which increases particle concentration near the wall. A higher particle concentration near the wall enhances particle deposition and, hence, diffusion loss (Hinds 1999). Wells and Chamberlain (1967) investigated the deposition

of 0.17–5 μm particles in the turbulent flow regime ($\text{Re} \approx 2000$ –50,000) on a center rod inside a tube experimentally. They derived the following equation for the deposition velocity v_d of particles, which is defined as the particle flux to the wall divided by the number concentration of particles in the bulk flow:

$$v_d = \frac{0.039u_0}{\text{Re}^{1/4}} \left(\frac{\rho_g D}{\eta} \right)^{2/3} \quad (9)$$

$$\text{Re} = \frac{(d_1 - d_2)u_0\rho_g}{\eta}. \quad (10)$$

In this equation, u_0 denotes the superficial velocity, ρ_g denotes the gas density, and d_1 and d_2 denote the outer and inner diameter of the annular channel, respectively. The equation is experimentally verified for 0.17–0.65 μm particles and Re from 13,000 to 25,000 (Wells and Chamberlain 1967). The resulting penetration for particles in turbulent flow inside a tube is given by Lee and Gieseke (1994), using v_d from Eq. (9):

$$P = \exp\left(-\frac{4v_d L}{du_0}\right). \quad (11)$$

Although Wells and Chamberlain derived their equation for turbulent flow in an annular channel, Eq. (11) also describes the data of Kumar ($x = 5$ –100 nm; $\text{Re} = 461$ –1409) and Symonds ($x = 8$ –100 nm; $\text{Re} = 378$ –5038) for flow in cylindrical tubes very well (Kumar et al. 2008; Symonds et al. 2007) even in the laminar regime. It is remarkable that in the case of turbulent flow, the diffusion losses are dependent of the tube diameter in contrast to the laminar case. According to Wells and Chamberlain, the penetration increases with increasing tube diameter.

In sampling lines, tube expansion and reduction pieces may be necessary. Correlations for the calculation of particle losses in such expansion and reduction pieces are not known to the authors. The authors suppose that tube expansion and reduction pieces can lead to secondary flows which transport particles from the core of the flow further towards the walls and enhance deposition similar to the findings of Wang for bends and elbows (Wang et al. 2002). Beside these passages, the flow velocity profile has to develop in each new tube with a different diameter. Chen and Comparin investigated the diffusion loss of particles in tubes during development of a Hagen–Poiseuille velocity profile out of a plug flow profile numerically (Chen and Comparin 1976). They showed that the influence of a developing flow profile on diffusive losses can be neglected when the Schmidt number Sc is above 100:

$$\text{Sc} = \frac{\eta}{\rho_g D}. \quad (12)$$

Besides the tubing, the wire mesh at the aerosol inlet acts as an additional particle collector. Cheng and Yeh derived an equation for the penetration of particles through several screens of parallel cylinders in the diffusion deposition regime (Cheng and Yeh 1980):

$$P = \exp(-APe^{-2/3}) \tag{13}$$

$$A = \frac{2B\alpha}{\pi(1-\alpha)r}h \tag{14}$$

$$Pe = \frac{2ru_0}{D} \tag{15}$$

In this equation, α denotes the solid volume fraction of the mesh, r denotes the wire radius, and h denotes the thickness of the wire mesh. The parameter B is given as 2.7 for the fan model (Cheng and Yeh 1980) which is applicable for the wire mesh. The single-fiber collection efficiency used in this theory is based on Kirsch and Fuchs work who measured the penetration of particles through diffusion batteries and filters (Kirsch and Fuchs 1968). Cheng and Yeh indicate that their equation is valid for particles from 0.005 to 0.2 μm (Cheng and Yeh 1980), but Alonso measured according penetrations even for particles as small as 2 nm (Alonso et al. 1997).

Electrical particle charge can cause additional losses due to electrostatic dispersion, image force, or precipitation in electric fields.

Unipolarly charged particles repulse each other, which lead to an expansion of unipolar charged aerosol clouds and thus deposition of particles on tubing walls. The particle penetration through tubes due to electrostatic dispersion and diffusion losses can be calculated according to Alonso and Alguacil (2007):

$$P = \frac{P_{\text{diffusion}}}{1 - 0.46v_s(1 - P_{\text{diffusion}})/\ln(P_{\text{diffusion}})} \tag{16}$$

$$v_s = \frac{ne^2c_{\text{in}}LC_c}{3\pi\eta x u_0 \epsilon_0} \tag{17}$$

$P_{\text{diffusion}}$ denotes the penetration due to diffusion, v_s denotes the dimensionless particle velocity due to electrostatic dispersion, n denotes the number of elementary charges per particle, e denotes the elementary charge of $1.602176634 \times 10^{-19}$ C (NIST Standard Reference 2019), and ϵ_0 denotes the electric permittivity of air of 8.85959×10^{-12} F/m (NIST Standard Reference 2019; Hector and Schultz 1936).

Charged particles near conductive surfaces influence electron movements in the conductor causing attractive forces, the so-called image forces. Particle deposition by

image force in tubes can be calculated according to Yu and Chandra (1978):

$$\frac{(ne)^2}{48\pi^2\eta x \epsilon_0 u_0 \left(\frac{d}{2}\right)^3}L = 2 \left[\frac{d}{d_c} + 2\ln\left(\frac{d_c}{d}\right) - \left(\frac{d_c}{d}\right)^2 + \frac{1}{3}\left(\frac{d_c}{d}\right)^3 - \frac{1}{3} \right] \tag{18}$$

$$P = 1 - \left[1 - \left(\frac{d_c}{d}\right)^2 \right]^2; \tag{19}$$

with the diameter d_c out of which all particles are deposited on the tube walls due to image force. This diameter has to be determined by solving the implicit equation [Eq. (18)] iteratively.

The third mechanism which can cause electrostatic particle loss is by Coulomb forces of charged particles in an electric field. Such fields can result from surface charges of the surrounding tubing, which are most likely present on insulating materials. Liu et al. used a simple formula for the penetration of particles through tubing with electric fields, or for the calculation of an effective electric field strength using data from penetration measurements (Liu et al. 1985):

$$P = \exp\left(-\frac{\pi dLE}{V} \frac{neC_c}{3\pi\eta x}\right) \tag{20}$$

Entire sampling systems often consist of a serial arrangement of different components. The total penetration P_{ges} through a system that contains k different components in series can be calculated by multiplication of the individual component penetrations $P_i(x)$:

$$P_{\text{ges}}(x) = \prod_{i=1}^k P_i(x) \tag{21}$$

2 Materials and Methods

2.1 Experimental Setup

2.1.1 Sampling System

To measure particle loss of the sampling system or single components of it, a test aerosol must be generated and lead through the sampling line. Measurements of the concentration of particles with a certain size upstream and downstream the sampling system allow determination of the particle loss and the particle penetration.

The sampling head was glued inside a metal bucket with an inner diameter of 32 cm and an inner height of 39 cm to expose it to the test aerosol without causing emissions of the



Fig. 2 Sampling head and cap of the metal bucket

test aerosol to the environment. Figure 2 shows the sampling head with the cap of the metal bucket. The distance from the top of the head to the bucket head was 19.8 cm. The aerosol inlet was on the same axis as the sampling head and 19.2 cm above it. The upstream sample was taken from a hole in the cap of the bucket 55 mm apart from the side of the sampling head. Additionally to exposing the sampling head to the test aerosol, the metal bucket compensated fluctuations in the aerosol number concentration over time due to his volume of 31.4 dm³.

To measure the losses of the entire sampling system, the bucket was installed upside down on the IADS, which was fitted on top of the nafion-dryer. The aerosol in the nafion-dryer flowed countercurrent to the shell-side dry air. Figure 3 depicts the entire sampling system.

2.1.2 Aerosol Generation and Characterization

Test particles for measurement of losses are generated in a custom-built spark-discharge generator (see Fig. 4). The generator contains two copper electrodes with a diameter of 5 mm, which are placed 3 mm apart from each other in a parallel circuit with a 0.0063 μF capacitor and a high voltage–power supply (HCK 400 M–20,000, manufacturer FuG Elektronik GmbH). The generated aerosol is diluted and passes two vessels with a volume of 6.2 dm³ each to reduce particle concentration fluctuations over time. The aerosol is then led through a tube furnace (MTF 12/25/400, manufacturer Carbolite Gero GmbH & Co. KG). The purpose of this tube furnace is to coalesce the copper agglomerates into single spheres, so that the Stokes–Einstein equation can be used to calculate their diffusion coefficient (Eq. 5).

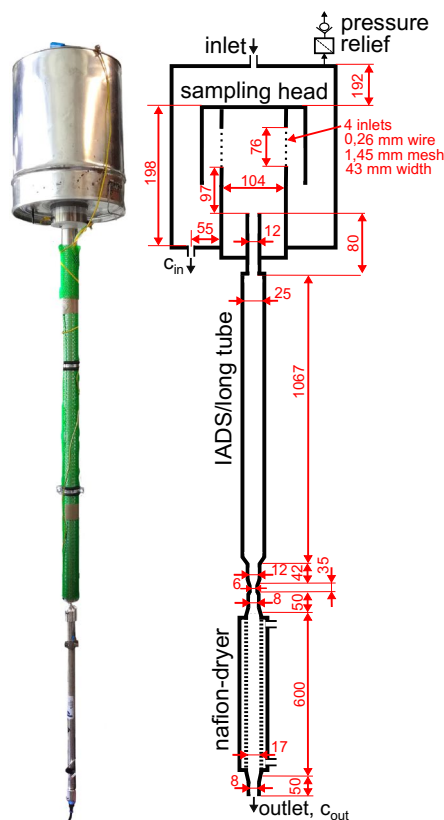


Fig. 3 Sampling system containing the sampling head inside a metal bucket, the IADS, and the nafion-dryer. All dimensions in mm

To evaluate the test particles by transmission electron microscopy (TEM), a custom-made low-pressure impactor with a nozzle diameter of 2 mm was used according to Fig. 5. An impaction plate with a fixture for TEM grids was placed 1 mm downstream of the nozzle. The flow is sucked through the impactor by a vacuum pump (DUO 20M, manufacturer Pfeiffer Vacuum GmbH) and adjusted with a critical orifice. With this setup, samples of the particles are collected for TEM analysis of the shape and size of the aerosol particles.

2.1.3 Penetration Measurements

To determine the penetration of particles through a test section, the number concentration of particles with a certain size must be measured upstream and downstream the test section. The test section can consist of the whole sampling line or single components of the sample line. Figure 6 shows three variants of the experimental setup used to determine the penetration through a test section.

In the setup shown in Fig. 6a, the test aerosol first flows through the inlet impactor and the neutralizer of a Scanning Mobility Particle Sizer control unit (SMPS) (DEMC X control unit, manufacturer Palas GmbH). Coarse particles are

Fig. 4 Copper-nanoparticle–aerosol generation by spark discharge and sintering inside a tube furnace

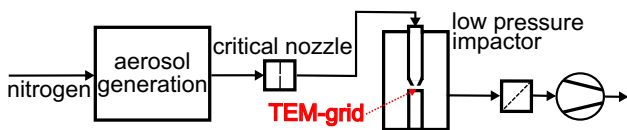
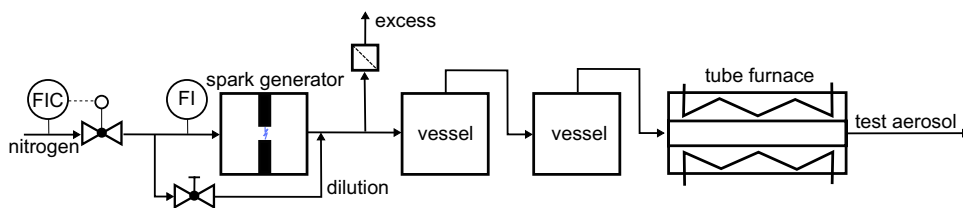


Fig. 5 Setup to sample the generated aerosol on TEM grids

removed in the impactor and the copper nanoparticles are electrically neutralized by soft X-ray radiation inside the control unit and classified by a Differential Mobility Analyser (DMA) (DEMC 2000 column, manufacturer Palas GmbH) according to their electrical mobility. The size-selected test aerosol flows through a vessel of 143 cm³ and into the test section. Aerosol concentrations can be measured upstream and downstream of the test section by a Condensation Particle Counter (CPC) (ENVI-CPC 100, manufacturer

Palas GmbH). The tubing from the sample points to the CPC is electroconductive and the test section is grounded to reduce particle deposition due to electrostatic forces. Both sampling lines from the test section to the CPC have equal length and, hence, identical particle penetrations, so that the ratio of the measured number concentrations downstream and upstream the test section gives the penetration through the test section alone. The valves were made of short parts of rubber tubing with tube clamps. The rubber tubing has equal length and, hence, particle penetration. This was confirmed experimentally.

The advantage of classifying the aerosol upstream the test section is the quick response of the CPC signal to switching the sampling position, which reduces influences of shifts in particle generation on the determined penetration. Another advantage is the known charge

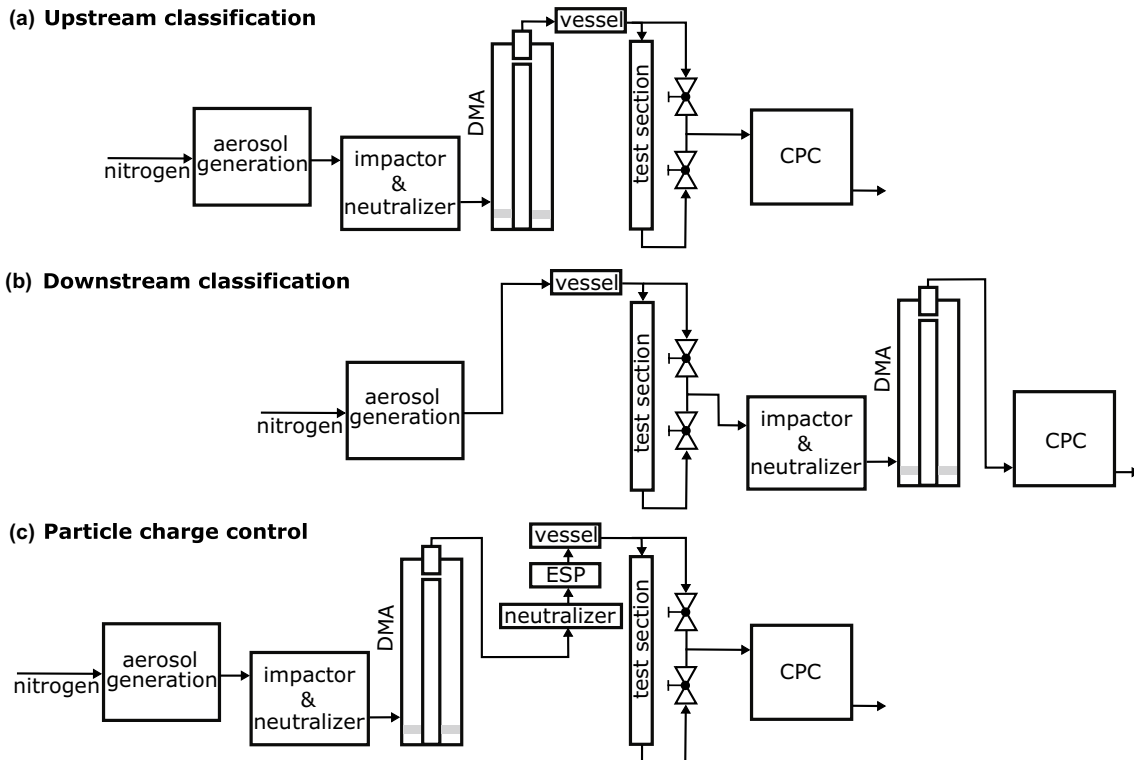


Fig. 6 Setups for measurement of the penetration through a test section. Classification of the copper nanoparticles can take place before (a) or after the test section (b), and the influence of the particles electrical charge can be determined with an additional neutralizer and ESP (c)

distribution of the aerosol after electrical neutralization and classification.

A variation of this setup is shown in Fig. 6b. The difference to the Fig. 6a is that aerosol with a broader size distribution flows through the test section. Aerosol is sampled upstream and downstream the test section and the number concentration of particles with a certain size is measured by a complete SMPS system. The SMPS was operated in classifier mode and thus with a constant voltage analogous to the setup in Fig. 6a.

The advantage of classifying after the test section is that particles that enter the system through leaks upstream the test section are classified too, so that the determined penetration is associated with the correct particle size. This was necessary in measurements in which the test section contains the Sigma-2-Sampling head, because the sampling head was glued in a metal bucket which was not leak-proofed. This means that small amounts of environmental air may enter the system upstream the test section and serve as additional test aerosol, which must be classified afterwards. The metal bucket can be represented by the vessel in Fig. 6b, because it is upstream the sampling system and reduces fluctuations in particle concentration. A further advantage is that measuring times are reduced for large volume test sections, because the test section is filled with a polydisperse aerosol and there is no time needed to flush it with a new particle size like in the setup, as shown in Fig. 6a.

A disadvantage of this setup is the unknown charge of the particles in the test section, because electrical neutralization of the aerosol only takes place in the neutralizer downstream the test section. Although the influence of particle charge on the penetration through electrical conductive and grounded tubes and wire mesh is negligible for neutralized/singly charged particles (Alonso et al. 1997), thermionic emissions in the tube furnace may produce particles with multiple charges (Magnusson et al. 1999) which might decrease penetration efficiency measured with this setup.

The setup in Fig. 6c is similar to (a) and contains an additional ^{85}Kr -neutralizer and an Electrostatic Precipitator (ESP) to determine the influence of the particle charge on penetration. The self-built ESP consists of a center rod with a diameter of 30 mm inside a pipe with an inner diameter of 50 mm. The precipitation length is 150 mm. The penetration of particles with a single unipolar charge can be measured with the DMA upstream the test section (Fig. 6a), while the penetration of uncharged and electrically neutralized particles can be measured with the setup in Fig. 6c if the voltage in the ESP is high or zero, respectively. An ESP voltage of 5.001 kV was applied to produce the uncharged aerosol. This voltage should precipitate all singly charged particles smaller than 600 nm.

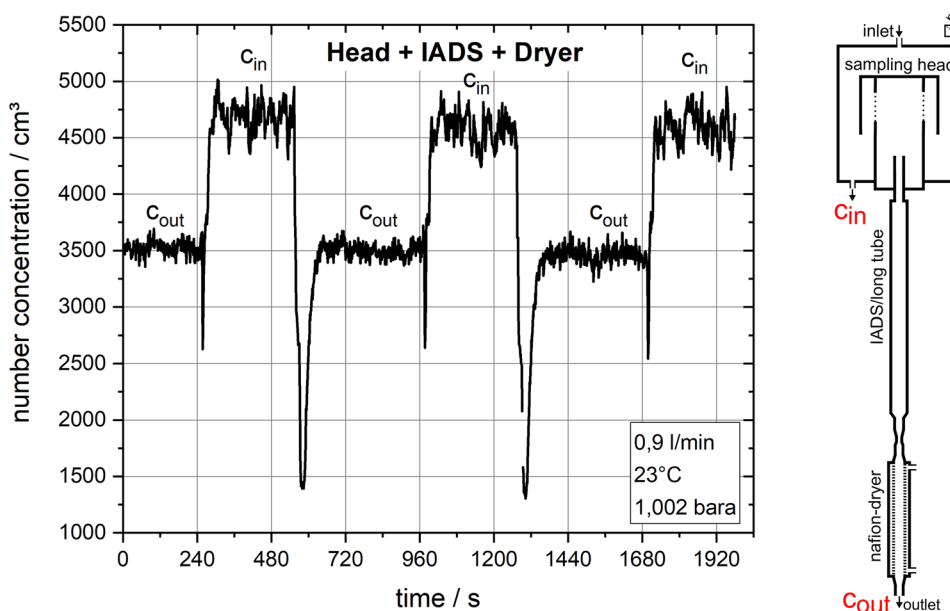
2.2 Measurement Procedure and Data Analysis

In all experiments, the voltage between the spark generator electrodes was 3.4–4.1 kV and the electric current which loads the capacitor parallel to the electrodes was 0.6 mA. Around 6.8 l of nitrogen per minute at standard conditions (273.15 K, 1.000 bar) flowed through the spark generator and around 17.6 additional liters of nitrogen were added downstream of the spark generator to reduce particle agglomeration by collision. The dilution factor was 3.6. The tube furnace was operated at a temperature of 850 °C and the flow through the CPC was set at 0.9 l per minute. The ratio of sheath-to-aerosol volume flow rate in the DMA was 5:1. The resulting mean particle concentrations for monodisperse aerosol upstream the test section were 582 #/cm³, 1814 #/cm³ and 3133 #/cm³ for 10 nm, 15 nm and 20 nm, respectively, in the setup, as shown in Fig. 6a. In the similar setup shown in Fig. 6c, these particle concentrations were 411 #/cm², 1479 #/cm³, and 2415 #/cm³ for 10 nm, 15 nm, and 20 nm particles, respectively. In the setup shown in Fig. 6b, the mean particle concentrations upstream the test section were 1752 #/cm³, 4656 #/cm³, 7206 #/cm³, and 5983 #/cm³ for 10 nm, 15 nm, 20 nm, and 40 nm, respectively. The higher particle concentration in setup (c) was caused by additional aerosol, which enters the bucket through leakages, and different flow conditions upstream the metal bucket, which were caused by the pressure relief in the metal bucket.

To investigate the penetration of particles with a certain size, the particle concentration was measured alternately upstream and downstream of the test section. Figure 7 exemplarily shows the measured number concentration of 15 nm particles over time for one experiment. The measurements were done with the setup presented in Fig. 6b and show that the concentration upstream the sampling system was about 4600 #/cm³, and downstream about 3500 #/cm³. To determine the penetration of one particle size, a series of three upstream and three downstream measurements was taken. The concentrations in these intervals were averaged over the last 4 min, while the first 1–3 min after switching between the sample points were discarded.

Penetrations \bar{P}_i were calculated from consecutive downstream and upstream measurements. The standard deviation of the mean concentration $\Delta\bar{c}_i$ of the 10-s values of the evaluated 4 min was calculated and used to determine the standard deviation of the mean penetration $\Delta\bar{P}_i$ of the according measurement interval with Gaussian error propagation. $\Delta\bar{P}_i$ was then used to calculate a weighed mean penetration and a weighed mean standard deviation of the weighed mean penetration for a series of successive penetration measurements (Ghaffarpasand et al. 2012):

Fig. 7 1-s average of 15 nm particle concentration measured by the CPC over time. The concentration was measured upstream and downstream the entire sampling system



$$\bar{P} = \frac{\sum_{i=1}^n \frac{\bar{P}_i}{\Delta \bar{P}_i^2}}{\sum_{i=1}^n \frac{1}{\Delta \bar{P}_i^2}} \quad (22)$$

$$\Delta \bar{P} = \frac{\sum_{i=1}^n \frac{\Delta \bar{P}_i}{\Delta \bar{P}_i^2}}{\sum_{i=1}^n \frac{1}{\Delta \bar{P}_i^2}} \quad (23)$$

Using this procedure, the penetrations with the lower standard deviation are weighed stronger. $2\Delta \bar{P}$ is used for the error bars in Sect. 3.

Additional errors are caused by the uncertainty of the concentration measurement of the CPC (5% according to the manufacturer). Another source of uncertainty is shifts in the aerosol concentration caused by its production and different particle losses in the fittings upstream and downstream the sample line. To determine these different particle losses, the upstream sampling point and the downstream sampling point were connected together directly, leading to a 2% deviation from the ideal penetration of 100%. The influence of the particles electric charge was investigated for the dryer in more detail and should be low for the other components, because they are grounded and electrical conductive. Nevertheless, electrostatic effects can lead to lower particle penetrations compared to the penetrations for pure diffusion in all components.

3 Results and Discussion

In this section, first, the aerosol is characterized by TEM images. Second, the penetration through a simple tube is determined with the setup shown in Fig. 6a for

direct comparison with literature and verification of the experimental setup. Third, the penetrations through the components of the test section are investigated bottom-up, starting with the nafion-dryer and a detailed study on the influence of particle charge on penetration. Then, the IADS is added to the nafion-dryer and penetrations are determined using the setup in Fig. 6a. The penetration of the IADS alone is calculated from the penetration through the nafion-dryer and the penetration through nafion-dryer and IADS in series using Eq. (21). Finally, the penetration through the entire sampling system consisting of nafion-dryer, IADS, and sampling head is measured using the setup, as shown in Fig. 6b. The penetration through the sampling head is calculated from these data and compared to the penetration measured through the sampling head alone (using the setup in Fig. 6b) to verify the method of calculating penetrations by using Eq. (21).

Figure 8 shows TEM images of the copper nanoparticles used for the measurement of the particulate losses inside the sampling line. The volume flow through impactor and tube furnace was 1.0 l per minute at standard conditions and particles from the aerosol were sampled on a TEM grid for 10 min.

The particles in Fig. 8 seem to be spherical and mostly unagglomerated, which allows the calculation of their diffusion coefficient by Eq. (5). There are some doublets which are bigger than the particles used for the measurements of diffusive losses. Although these doublets are bigger, they may pass the DMA with the monodisperse aerosol, if they carry multiple electric charges. This shows that the particles generated by spark discharge and sintering in a tube furnace are suited for the measurement of losses in the subsequent experiments.

Fig. 8 TEM images of the generated copper nanoparticles after sintering

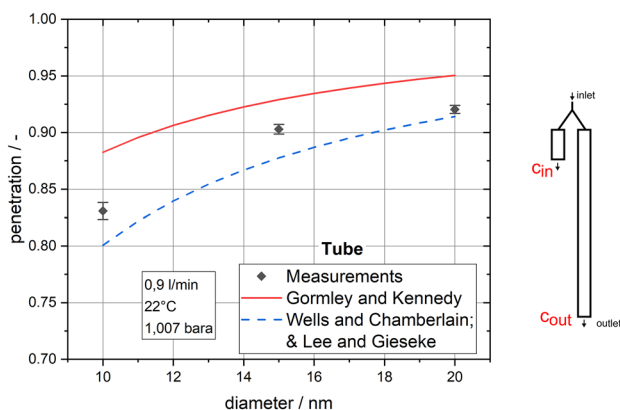
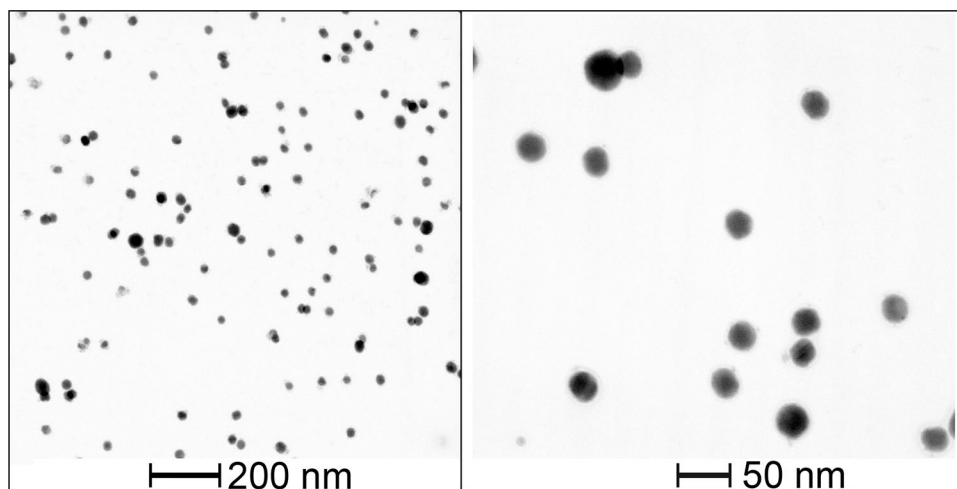


Fig. 9 Penetration through a tube of 3.9 mm inner diameter and an effective length of 99.1 cm at 0.9 l/min without inlet effects in comparison with the theories of Gormley and Kennedy (1948), Wells and Chamberlain (1967) and Lee and Gieseke (1994). Error bars denote $2\Delta\bar{P}$

The penetration of particles through a pipe of 3.9 mm inner diameter and a length of 1.141 m at 0.9 l per minute was measured with the setup in Fig. 6a to compare our measurements with results from literature. To eliminate inlet effects in the tube, the sample upstream of the 1.141 m tube flowed through a similar but somewhat shorter 0.15 m long tube before it reached the CPC. This means that the measured penetration corresponds to the penetration through a 99.1 cm tube without inlet effects. Additionally, because the Schmidt number was higher than 100 for every measured particle size, such inlet effects are considered to be negligible according to Chen and Comparin (1976). Figure 9 shows the results of this experiment.

The measured penetrations are found to be between the predictions by the diffusion loss theories for laminar flow (Gormley and Kennedy 1948) and turbulent flow (Wells and Chamberlain 1967; Lee and Gieseke 1994). The theory for

the turbulent flow seems to describe the measurements better, although the Reynolds number in the experiments was only 319 and, hence, the flow laminar. This finding is in accordance with the literature (Kumar et al. 2008; Symonds et al. 2007) where the theory for turbulent flow (Wells and Chamberlain 1967; Lee and Gieseke 1994) also seems to match measurement results better, and therefore, only the theory for turbulent flow is considered in the following discussion.

The impact of the nafion-dryer on particulate losses was investigated with the setup in Fig. 6a. In this experiment, there was no pressure difference between tube side and shell side of the nafion-dryer, and the volume flow rate of the aerosol was 0.9 l per minute. The results are shown in Fig. 10. Inlet and outlet diameters of the dryer are 8 mm and the total length measures 70 cm. The Nafion tube inside has an effective length of 60 cm and an inner diameter of 17 mm according to the manufacturer. The diffusion loss of a similar tube according to the theory for diffusion loss in turbulent flow (Wells and Chamberlain 1967; Lee and Gieseke 1994) is plotted as dashed line in Fig. 10.

The calculated penetration of a similar tube (dashed line) is higher than the actual measured penetration. To describe the measured penetrations, the diameter d_{eff} and length L_{eff} of a single tube with equal penetration according to Wells and Chamberlain (1967) and Lee and Gieseke (1994) are determined with the generalized reduced gradient algorithm implemented in MS Excel 2019. The fit equation is:

$$P = \exp \left(- \frac{4L_{\text{eff}}}{d_{\text{eff}}u_0} \frac{0,039u_0}{\left(\frac{d_{\text{eff}}u_0\rho_g}{\eta} \right)^{1/4}} \left(\frac{\rho_g D}{\eta} \right)^{2/3} \right). \quad (24)$$

An advantage of this fit equation in contrast to the theory of Gormley and Kennedy, when used as a basis for a fitting

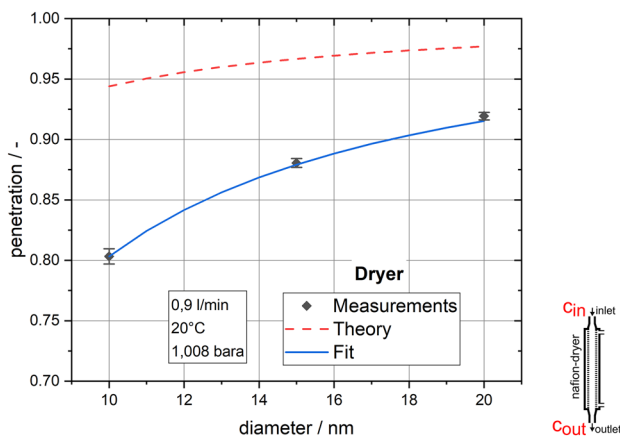


Fig. 10 Penetration through the nafion-dryer at 0.9 l/min. The continuous line shows a fit to the measurement results with an effective length of 1.660 m and an effective diameter of 7.9 mm according Eq. (24) (shown later). Theoretical calculation according to Wells and Chamberlain (1967) and Lee and Gieseke (1994)

equation, is the additional dependence of the penetration on the tube diameter. This tube diameter serves as second-fit parameter, in addition to the tube length, and considers the internal changing tube diameter of the dryer. The calculated equivalent diameter of the dryer is 7.9 mm and the equivalent length is 1.660 m.

Penetration measurements through the nafion-dryer were also performed by Bohensky et al. at the Leibniz Institute for Tropospheric Research (TROPOS) at higher flow rates (Bohensky et al. 2014). Figure 11 shows the data measured by Bohensky et al. at a flow rate of 2.0 l/min and the penetrations calculated using the correlation for the dryer from this study. All measured penetrations are higher than the penetrations expected by the correlation and differences decrease with increasing particle size. This shows that further measurements at different flow rates are necessary to develop a better correlation for the dryer. Additionally, different surface charges on the Nafion membranes and different particle electric charges in the experiments may cause different penetrations.

Investigations concerning the electrical particle charge were performed to understand the difference in measured and calculated penetration, as shown in Fig. 10. Therefore, the whole setup was built up again 5 months after the original measurements. The downward pointing triangles in Fig. 12 show the penetrations determined with a setup similar to that used in Fig. 10. The maximal deviation to the former measurements is 0.02.

The penetrations of singly negative charged particles were determined by upstream classification of the particles in a DMA (Fig. 6a). The lowest penetrations were measured for this charge state. Completely uncharged particles were produced by precipitation of all charged particles inside an ESP

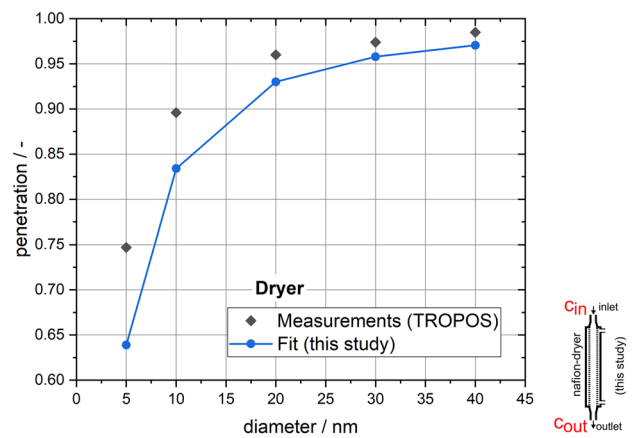


Fig. 11 Penetration through the nafion-dryer at 2.0 l/min. The fit was performed with an effective length of 1.660 m and an effective diameter of 7.9 mm determined in this study and the according fit equation [Eq. (24)]. Measurements were performed by Bohensky et al. (2014)

upstream the test section (Fig. 6c). The uncharged particles had the highest penetration through the dryer. Particles were neutralized for the measurements with an additional ⁸⁵Kr-neutralizer upstream the test section (Fig. 6c with an ESP voltage of 0 V). The neutralized particles have penetrations between those of charged and uncharged particles. Untreated particles are those at the outlet of the tube furnace (Fig. 6b) and they have also penetrations between those of the charged and the uncharged particles.

These measurements show a big influence of particle charge on penetration through the nafion-dryer. Penetrations due to electrostatic dispersion (Eq. 16), image force (Eq. 19), and electric fields by surface charges (Eq. 20) were calculated to determine the relevant deposition

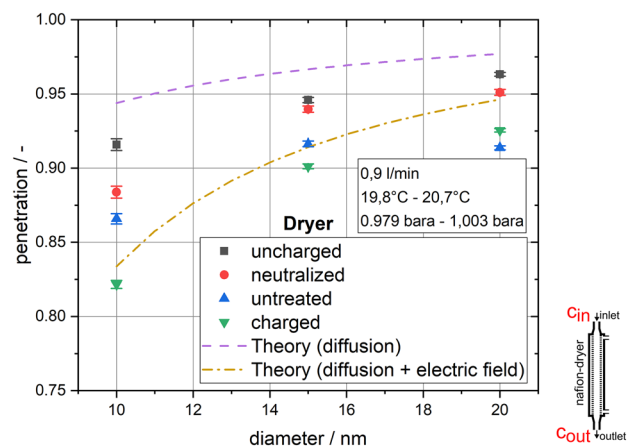


Fig. 12 Penetration through the nafion-dryer at 0.9 l/min. The electric charge of the particles was varied using the different setups shown in Fig. 6. Theoretical calculation according to Wells and Chamberlain (1967), Lee and Gieseke (1994), and Liu et al. (1985)

mechanism. Electrostatic dispersion and image force both result in particles losses less than 1.2% and are, therefore, not able to explain the difference in penetration of charged and uncharged 10 nm particles of almost 10%. These both mechanisms can, therefore, be neglected in the further study. An effective electric field causing the different particle loss of charged and uncharged particles was calculated for a mean tube diameter of 15.7 mm according to Eq. (20). An effective electric field strength of as low as 0.24 V/cm is able to explain this difference. The effective field strength of 0.24 V/cm is low in comparison to an effective field strength of 100 V/cm for Teflon and Polyflo tubing according to Liu et al. (1985), and could be caused by surface charges of the Nafion membrane. The electrical resistivity of Nafion of 570 Ω m at 33% relative humidity is rather low and increases with decreasing relative humidity (Opekar and Svozil 1995). Dry nitrogen was used in this experiments resulting in a higher electrical resistivity of the membrane, which enhances the presence of surface charges on the Nafion membrane. A higher relative humidity reduces the electrical resistivity of the membrane and may, therefore, reduce surface charges and particle deposition due to Coulomb forces. All other parts of the sampling system are conductive and grounded, and therefore, also Coulomb forces may be neglected in the further study.

The next part of the sampling system is the IADS. The IADS was inactive during the experiments, which means that it was not heated and was measured in series with the diffusion dryer using the setup in Fig. 6a. The penetration through the IADS alone can be calculated from the penetration through the nafion-dryer and the penetration through nafion-dryer plus IADS using Eq. (21). The results are shown in Fig. 13.

The IADS has a length of 123 cm and an inner diameter of 12 mm at inlet and outlet, respectively. Inside the IADS, the tube expands, but the exact geometry is unknown to the authors. This could explain the differences between the measured penetrations and the penetrations calculated for a similar tube (dashed line). The small differences between the measured penetrations and those calculated for diffusional deposition of particles in turbulent pipe flow (Wells and Chamberlain 1967; Lee and Gieseke 1994) may show the little influence of the electrostatic deposition mechanism in this part of the sampling system. An equivalent diameter of 18.1 mm and an equivalent length of 124.5 mm result in the fit (continuous line) shown in Fig. 13 according to Eq. (24).

The measured data for dryer and IADS in series are plotted in Fig. 14. In this experiment, there was no pressure difference between tube side and shell side of the nafion-dryer. The line is a fit with Eq. (24) and the respective equivalent lengths and diameters of IADS and dryer determined above.

The final part of the sampling system in our investigations is the Sigma-2-Sampling head. The head was investigated

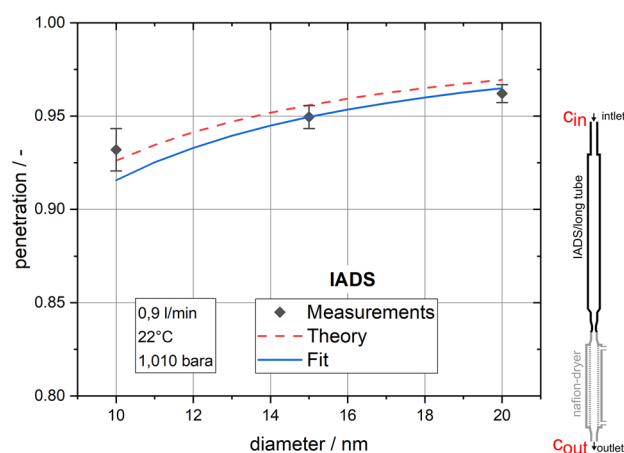


Fig. 13 Penetration through the IADS at 0.9 l/min. A fit to the measured data is done with Eq. (24) and an equivalent diameter of 18.1 mm and an equivalent length of 124.5 cm. Theoretical calculation according to Wells and Chamberlain (1967) and Lee and Gieseke (1994)

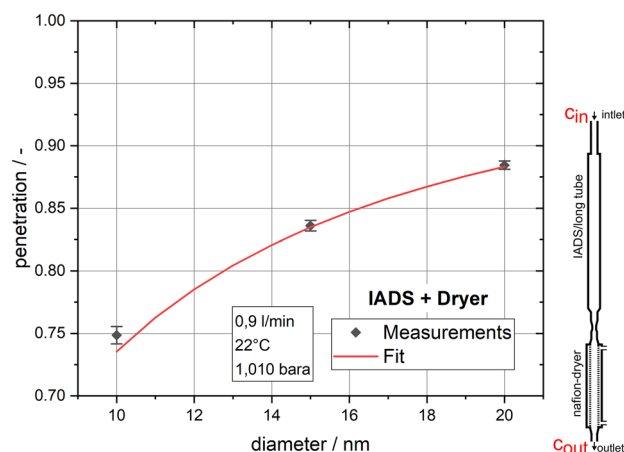


Fig. 14 Penetration through IADS and dryer in series at 0.9 l/min. The continuous line is a fit with the determined equivalent diameters and lengths of the both components in combination

together with the dryer and the IADS in series using the setup shown in Fig. 6b. Penetration through the head alone is calculated with Eq. (21) and shown in Fig. 15.

The calculated penetration (Cheng and Yeh 1980) for neutral particles through a wire mesh with the same geometry is much lower than the measured penetration. The particles in the experiments were not electrically neutral; however, charged particles would have a higher collision efficiency on the grounded grid and, therefore, the penetration for charged particles would be even lower. Thus, electrostatic effects give no explanation for the deviation between theory and experiment. The influence of the flow velocity on the calculated penetration is high according to parameter variations. Because of this influence, it is supposed that inhomogeneous

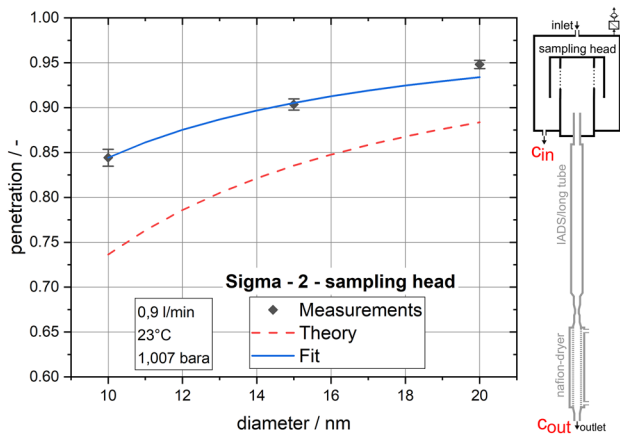


Fig. 15 Penetration through the Sigma-2-Sampling head at 0.9 l/min. The continuous line is a fit to the measured data using Cheng and Yeh’s theory and an equivalent parameter A of 0.692 defined by Eq. (14)

flow conditions are responsible for the higher measured penetration. The measured data were fitted with the theory of Cheng and Yeh and an equivalent parameter of $A = 0.692$ where $A = 0.923$ was calculated for the geometry of the wire mesh using Eq. (14).

The sampling head was also measured alone because of the large differences of measurement and calculation. The penetrations determined by measurement of the sampling head alone and by measurement of the whole sampling line are shown in Fig. 16. The differences in these penetrations are small and proof the experimental procedure.

Finally, the entire sampling system consisting of nafion-dryer, IADS, and sampling head was investigated with the setup shown in Fig. 6b. The results are plotted in Fig. 17.

In this experiment, also the pressure difference between the tube-side aerosol and the shell-side dry air in the nafion-dryer was varied between 0 and 70 kPa. Additionally, the penetration of 40 nm particles was measured in this experiment to show the small diffusive losses of bigger particles. The continuous line shows a fit with the equivalent parameters calculated for the single components according to Wells and Chamberlain, Lee and Gieseke, and Cheng and Yeh. The measured penetration of 10 nm particles is about 63% which means that more than 30% of the 10 nm particles are lost in the sampling system. Because 7 nm particles will have an even lower penetration of 48%, as predicted by the fit function, the sampling system will not fulfill a minimum penetration of 70% for 7 nm particles as specified in DIN CEN/TS 16976 (DIN CEN/TS 16976 2016).

Based on the assumption that the penetration through sampling head and IADS is independent of the difference pressure in the dryer, a new equivalent diameter of 7.61 mm and an equivalent length of 1.487 m were determined for the dryer at the pressure difference of 70 kPa.

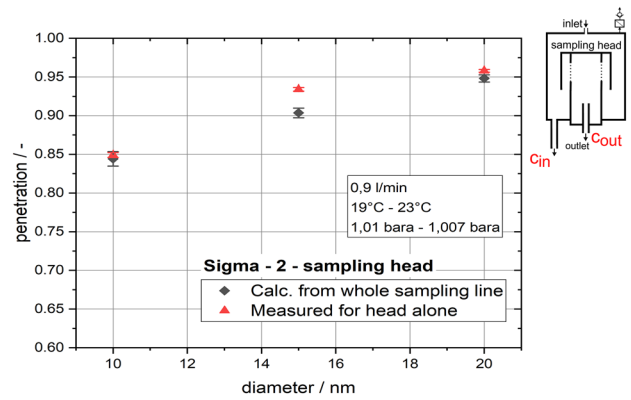


Fig. 16 Penetration through the Sigma-2-Sampling head at 0.9 l/min. Triangles show penetrations determined by measurements of the sampling head alone and diamonds those calculated out of the measured penetrations for the entire sampling line

The pressure difference in the nafion-dryer has a small influence on particle penetration and results in slightly higher penetrations for 70 kPa. A possible explanation for the higher penetrations at increased pressure difference is leakages inside the dryer, which causes aerosol to leave the sampling line and thus results in a bigger volume flow rate upstream the dryer.

The fit functions with the equivalent parameters which were fitted to the penetration of 10, 15, and 20 nm particles are not able to extrapolate to bigger particles, because the measured penetration for 40 nm particles is significantly higher than the extrapolations.

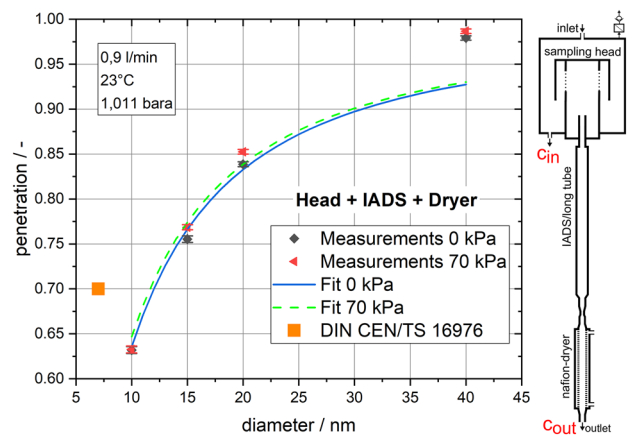


Fig. 17 Penetration through the complete sampling system for two values of the pressure difference across the Nafion membrane in the dryer at 0.9 l/min

4 Conclusion

In this study, the penetration of 10, 15, and 20 nm particles through a sampling system consisting of a probe head (Sigma-2-Sampling head, manufacturer Palas GmbH), a long pipe (IADS, manufacturer Palas GmbH), and a nafion-dryer (MD-700-24S-1, manufacturer Perma Pure LLC) was investigated at a flow rate of 0.9 l/min. The sampling system, therefore, consists of components interchangeable with those of sampling lines for measurement of fine particulate matter and has a low-energy consumption because of the low flow rate. The following results were achieved:

- Test aerosol containing single spherical particles was produced by spark discharge and sintering of the resulting agglomerates. The shape of the particles was evaluated with TEM measurements.
- The theory of Wells and Chamberlain (1967) and Lee and Gieseke (1994) describes measured penetrations through a tube at laminar flow conditions better than the theory of Gormley and Kennedy (1948), although it was derived for turbulent flow.
- Increasing pressure difference between the tube-side aerosol and the shell-side dry air in a nafion-dryer slightly increases the penetration.
- The particle loss of singly charged particles in the nafion-dryer is higher than that of uncharged particles. The higher particle losses may be caused by an effective electric field of 0.24 V/cm resulting from surface charges of the Nafion membrane.
- The diffusion loss of 10 nm particles through the whole system is about 37%. The nafion-dryer has the highest share with 20% particle loss.
- A fit function based on the theories of Wells and Chamberlain (1967), Lee and Gieseke (1994), and Cheng and Yeh (1980) was derived to describe the determined penetrations through the sampling system.
- Extrapolation of the determined equation suggests that the sampling system has a lower penetration for 7 nm particles than specified in DIN CEN/TS 16976 and, therefore, needs to be considered in environmental measurements of ultrafine particles.

Further investigations are necessary addressing the following subjects:

- Influence of humidity and volume flow rate on particle penetration through the sampling system.
- Computational fluid dynamic simulations of the probe head to investigate the difference between measured penetration of particles through the wire mesh and the theory of Cheng and Yeh (1980).

- Penetration study with different sampling systems, which are build according to (DIN CEN/TS 16976 2016).
- Investigation on reduction of surface charges in the nafion-dryer.

Acknowledgements Open Access funding provided by Projekt DEAL. We gratefully acknowledge Dr. Harald Creutzmacher and the Landesanstalt für Umwelt Baden-Württemberg (LUBW) for the provision of the U-SMPS 2100X, the Sigma-2-Sampling head, the IADS, and the nafion-dryer.

Compliance with Ethical Standards

Conflict of interest This study was performed during the master thesis of Jonas Gulden, which was jointly supervised by the Karlsruhe Institute of Technology (KIT) and the Landesanstalt für Umwelt Baden-Württemberg (LUBW). The authors follow no commercial interests with this study. On behalf of all authors, the corresponding author states that there is no conflict of interest.

Open Access This article is licensed under a Creative Commons Attribution 4.0 International License, which permits use, sharing, adaptation, distribution and reproduction in any medium or format, as long as you give appropriate credit to the original author(s) and the source, provide a link to the Creative Commons licence, and indicate if changes were made. The images or other third party material in this article are included in the article's Creative Commons licence, unless indicated otherwise in a credit line to the material. If material is not included in the article's Creative Commons licence and your intended use is not permitted by statutory regulation or exceeds the permitted use, you will need to obtain permission directly from the copyright holder. To view a copy of this licence, visit <http://creativecommons.org/licenses/by/4.0/>.

References

- Alonso M, Alguacil FJ (2007) Penetration of aerosol undergoing combined electrostatic dispersion and diffusion in a cylindrical tube. *J Aerosol Sci* 38:481–493. <https://doi.org/10.1016/j.jaerosci.2007.03.001>
- Alonso M, Kousaka Y, Hashimoto T, Hashimoto N (1997) Penetration of nanometer-sized aerosol particles through wire screen and laminar flow tube. *Aerosol Sci Technol* 27:471–480. <https://doi.org/10.1080/02786829708965487>
- Bohensky G, Sunada C, Smith P, Wiedensohler A, Tuch T (2014) Characterizing the particle losses of a large diameter Nafion® Dryer. <https://www.permapure.com/wp-content/uploads/2014/06/MD-700-TROPOS-Presentation-10-2014.pdf>. Accessed 03 Dec 2019
- Chen RY, Comparin RA (1976) Deposition of aerosols in the entrance of a tube. *J Aerosol Sci* 7:335–341
- Cheng YS, Yeh HC (1980) Theory of a screen-type diffusion battery. *J Aerosol Sci* 11:313–320
- DIN CEN/TS 16976 (2016) Außenluft: Bestimmung der Partikelanzahlkonzentration des atmosphärischen Aerosols. Beuth Verlag GmbH, Berlin, p 58
- Ghaffarpassand O, Drewnick F, Hosseiniebalam F, Gallavardin S, Fachinger J, Hassanzadeh S, Borrmann S (2012) Penetration efficiency of nanometer-sized aerosol particles in tubes under turbulent flow conditions. *J Aerosol Sci* 50:11–25. <https://doi.org/10.1016/j.jaerosci.2012.03.002>

- Glassman I, Harris BL (1952) Collision diameters of some gases as a function of temperature. *J Phys Chem* 56:797–799. <https://doi.org/10.1021/j150498a036>
- Gormley PG, Kennedy M (1948) Diffusion from a stream flowing through a cylindrical tube. *Proc R Ir Acad Sect A Math Phys Sci* 52:163–169
- Hector LG, Schultz HL (1936) The dielectric constant of air at radiofrequencies. *Physics* 7:133–136. <https://doi.org/10.1063/1.1745374>
- Hinds WC (1999) *Aerosol technology: properties, behavior, and measurement of airborne particles*, 2nd edn. Wiley, New York
- Kirsch AA, Fuchs NA (1968) Studies on fibrous aerosol filters—III: diffusional deposition of aerosols in fibrous filters. *Ann Occup Hyg* 11:299–304
- Kleiber M, Joh R (2013) Berechnungsmethoden für Stoffeigenschaften. In: Verein Deutscher Ingenieure (ed) *VDI-Wärmeatlas: Mit 320 Tabellen*, 11., bearb. und erw. Aufl. Springer, Berlin, pp 137–174
- Kumar P, Fennell P, Symonds J, Britter R (2008) Treatment of losses of ultrafine aerosol particles in long sampling tubes during ambient measurements. *Atmos Environ* 42:8819–8826. <https://doi.org/10.1016/j.atmosenv.2008.09.003>
- Lee KW, Gieseke JA (1994) Deposition of particles in turbulent pipe flows. *J Aerosol Sci* 25:699–709
- Liu BYH, Pui DYH, Rubow KL, Szymanski WW (1985) Electrostatic effects in aerosol sampling and filtration. *Ann Occup Hyg* 29:251–269
- Magnusson MH, Deppert K, Malm J-O, Bovin J-O, Samuelson L (1999) Gold nanoparticles: production, reshaping, and thermal charging. *J Nanopart Res* 1:243–251
- NIST Standard Reference Database (2019) CODATA Internationally recommended 2018 values of the fundamental physical constants. <https://physics.nist.gov/cuu/Constants/index.html>. Accessed 08 Jan 2020
- Opekar F, Svozil D (1995) Electric resistance in a Nafion® membrane exposed to air after a step change in the relative humidity. *J Electroanal Chem* 385:269–271
- Sinclair D, Countess RJ, Hoopes GS (1974) Effect of relative humidity on the size of atmospheric aerosol particles. *Atmos Environ* 8:1111–1117
- Stanier CO, Khlystov AY, Pandis SN (2004) Ambient aerosol size distributions and number concentrations measured during the Pittsburgh Air Quality Study (PAQS). *Atmos Environ* 38(20):3275–3284. <https://doi.org/10.1016/j.atmosenv.2004.03.020>
- Symonds JPR, Jason SO, Kingsley R (2007) Sample line efficiency measured with a real time particulate size spectrometer. In: AAAR 26th Annual conference, Reno, Nevada Poster presentation, September 24–28. https://www.researchgate.net/profile/Jonathan_Symonds/publication/267448226_Sample_Line_Efficiency_Measured_with_a_Real_Time_Particiulate_Size_Spectrometer/links/544f865d0cf26dda0891b614/Sample-Line-Efficiency-Measured-with-a-Real-Time-Particulate-Size-Spectrometer.pdf. Accessed 14 June 2019
- Wang J, Flagan RC, Seinfeld JH (2002) Diffusional losses in particle sampling systems containing bends and elbows. *J Aerosol Sci* 33:843–857
- Wells AC, Chamberlain AC (1967) Transport of small particles to vertical surfaces. *Br J Appl Phys* 18:1793–1799
- Yu CP, Chandra K (1978) Deposition of charged particles from laminar flows in rectangular and cylindrical channels by image force. *J Aerosol Sci* 9:175–180